Contributions to the Study of Coronary Arteries in CTA Images

by

Ricardo Alberto Corredor Jerez

Submitted in satisfaction of
the requirements for the degree of

Master EEAP - Parcours Systèmes et Images
and
Maestría en Ingeniería de Sistemas y Computación

SUPERVISORS
Marcela Hernández Hoyos
Maciej Orkisz

July 2012

"La perseverancia y el esfuerzo
siempre serán recompensados con el éxito ..."

Abstract

Cardiovascular diseases remain to be the first cause of mortality in the world. In order to detect and quantify lesions in coronary arteries, a conservative approach is commonly followed, beginning with the localization of coronary starting points (ostia) and the extraction of the vessel centerline. This data is usually required to perform the lumen segmentation and helps lesion detection and stenosis quantification tasks. Due to its social, medical, and academic interest, this thesis presents some contributions to the study of coronary arteries in computed tomography angiography images, specially in the centerline extraction and lumen segmentation steps.

First, we describe an axis extraction method developed in our team and we propose an algorithm to correct vessel centerlines in orthogonal planes to the vessel direction. New axes seemed to be better centered specially in healthy sections, but still having problems close to calcified plaques and bifurcations. Then, we present six lumen segmentation methods falling in two groups: classical and classification approaches. Best qualitative results were obtained by methods based on region-growing and 2D active contours. The study shows some difficulties to make a correct validation with the reference data, being one of the main reasons to obtain a low Dice score using k-means clustering (66.48%) which is comparable to the result obtained by a classic thresholding (65.20%). This is caused by the presence of some regions that make part of the vascular lumen ,e.g. a part near the aorta near the ostia, which are wrongly labelled as non-lumen sections. These regions are thus recognized as false positives.

Additionally, all the techniques present important drawbacks due to the difficulty in expressing an explicit geometrical model and a generic intensity profile of coronary arteries, specially in bifurcations and lesions. Trying to avoid this explicit modeling, we used Support Vector Machines, considered as a powerful generic classification method, but we obtained poor segmentation results with Dice scores under 50% and a considerable increase in computational costs during training phases. This is probably caused by a feature selection unsuited to describe the lumen. Finally, additional future efforts must be made in order to define a complete evaluation framework that permits the method's comparison and the complete analysis in coronary arteries.

Résumé

Les maladies cardiovasculaires demeurent la première cause de mortalité dans le monde. Pour détecter et quantifier les lésions dans les artères coronaires, l'approche classique est de commencer par localiser de points de départ des artères (ostia) et d'extraire la ligne centrale (axe) du vaisseau. Ces données sont nécessaires pour exécuter la segmentation du lumen vasculaire et elles aident à la réalisation des tâches suivantes comme la détection de lésions et la quantification de sténoses. En raison de l'intérêt social, médical et académique de ce sujet, ce mémoire présente quelques contributions à l'étude d'artères coronaires dans des images d'angiographie par tomodensitométrique, particulièrement dans l'extraction des axes et la segmentation du lumen.

Dans un premier temps, nous décrivons une méthode d'extraction des axes développée dans notre groupe et nous proposons un algorithme pour le recentrage des axes dans les plans orthogonaux à leurs directions principales. Après ce traitement, les nouveaux axes ont semblé être mieux centrés notamment dans le cas des sections saines, avec néanmoins des problèmes lorsque les axes présentent des plaques calcifiées ou des bifurcations. Suite à cela, nous présentons six méthodes de segmentation du lumen catégorisées dans deux groupes principaux: techniques classiques et techniques de classification. Les meilleurs résultats qualitatifs ont été obtenus par des méthodes basées sur des contours actifs et de la croissance de région. L'étude montre quelques difficultés pour faire une validation adéquate avec les données de référence, ce qui est une des raisons majeures qui fait que l'on obtient un score de Dice très bas en utilisant un algorithme des k-moyennes (66.48 %) score comparable aux résultats obtenus par un seuillage classique (65.20 %), Ceci est causé par la présence des régions faisant partie du lumen vasculaire e.g. une partie de l'aorte près de l'ostium, mais n'étant pas annotées comme telles. Ces régions sont donc reconnues comme des faux positifs.

Toutes les techniques de segmentation testées présentent des inconvénients importants en raison de la difficulté à exprimer un modèle géométrique explicite et un profil d'intensité générique des artères coronaires, particulièrement dans le cas de bifurcations et de lésions. Afin d'éviter cette modélisation explicite, nous avons utilisé la méthode de séparateurs à vaste marge, considérée comme une technique de classification puissante, mais nous avons obtenu des résultats faibles de segmentation avec un score Dice en dessous de 50% et une augmentation considérable de coûts informatiques pendant les phases d'entrainement. Ceci est probablement dû à une sélection de descripteurs inadaptée pour décrire le lumen. Finalement, des efforts supplémentaires doivent être faits pour définir un cadre d'évaluation complet qui permettrait la comparaison des méthodes et l'analyse des artères coronaires.

Acknowledgements

Firstly, I would like to thank my supervisors Marcela Hernández and Maciej Orkisz for their support, their patience, for all their advices, and specially for their continuous confidence in my work throughout these years of labor. I would also like to say a big "Thank you!" to Maria Alejandra Zuluaga for all her support, she makes part of the persons that I admire the most, including also Marcela and Maciej.

I would also like to thank professors José Tiberio Hernández and Olivier Bernard for having supported the development of my master's studies. To Leonardo Flórez for his recent contribution with the project and my document. To some institutions and their staff that have sponsored this work: Interfacultades, Colciencias, CMIRA Scolarships.

Maintenant, je voudrais dire merci à toutes les personnes de CREATIS (Xavier, Adeline – merci pour les corrections!, Claire, info–dev, chercheurs, doctorants, stagiaires, ...) qui m'ont permis de connaître un peu plus la vie du labo. Agradezco a mis amigos colombianos, especialmente Carlos, Vanessa, Alfredo, Eduardo, Halime, Daniela, Nicole, Jenny,... gracias por aguantarme en esos momentos tan difíciles y estresantes. Y a mis amigas mexicanas, por hacerme sentir siempre como si estuviera en mi casa.

Aunque son los últimos en esta lista, son y serán siempre los primeros y a quienes les debo más. Agradezco enormemente a mis padres y a mis hermanas, porque siempre están conmigo dandome toda la energía para lograr mis metas. También a Paola por ser siempre un apoyo enorme e incondicional. Mi familia, esto es especialmente para ustedes!!

Contents

List of Figures

Chapter 1

Introduction

This document presents some contributions in two active research topics that helps to understand and quantify cardiovascular diseases (CVD): artery lumen segmentation and plaque detection. This study was mainly focused in coronary arteries due to the social, medical, and academic interest around the world in this subject due to a very high morbidity and mortality related to the coronary heart disease.

The following subsections introduce the relevant medical context about arteries and their illnesses, the image acquisition techniques used for diagnosis, and the main challenges to extract relevant data. In Chapter 2, a revision of the most recent methods in these topics is presented. Chapter 3 and 4 summarize the methods used and their results. Finally, the conclusions of this work are collected in Chapter 5.

1.1 Medical Context

Cardiovascular diseases remain as the leading cause of death in the world. The World Health Organization (WHO) classifies them as the highest health problem with an alarming level (39%) of deaths (17 millions in 2008) caused by non-communicable diseases among people under age of 70, followed by respiratory and digestive diseases (30%), cancers (27%), and others (World Health Organization, 2011). The most common reason of heart attacks and cerebrovascular problems is the blockage of the main arteries caused by the development of the atherosclerotic plaque, which begins by an accumulation of fatty materials in the inner arterial wall layer, reducing the blood flow to myocardium or to the brain.

In order to have a reliable and efficient diagnosis, new imaging techniques have been developed to help radiologists and physicians in early detection and treatment monitoring of CVDs. Nevertheless, these tasks can be tedious, time-consuming and error-prone, even for experienced specialists, requiring the use of robust methods to extract the most important information about diseases and anatomical characteristics. Recent studies have demonstrated that the use of advanced vessel analysis software improves the assessment of vascular diseases and reduces the inter-observer variability (Di Carli and Hachamovitch, 2007, Biermann et al., 2012).

1.1.1 Arterial Anatomy and Vascular Diseases

Artery and vein wall has a layer structure composed by the *tunica adventitia* (outermost layer), the *tunica media* and the *tunica intima* (innermost layer). The interior of the vessel enclosed by the *tunica intima* is called the vessel lumen.

Coronary arteries supply the cardiac muscle (myocardium) with oxygenated blood. Two main coronary trees cover the left and right part of this muscle and they start at two locations called *ostia* (Figure 1.1). The right coronary tree has a principal branch which is usually referred to as the right coronary artery (RCA). On the other side, the left coronary tree begins with a thicker branch called the left coronary artery (LCA), but not too far it divides into the left anterior descending artery (LAD) and the left circumflex artery (LCX). This second tree has an important influence in the correct work of the left ventricle that is responsible for providing all the rest of the body with oxygenated blood. The diameter of coronary arteries varies between 6 mm at ostia locations and 0.5 mm at 20 cm from the starting point.

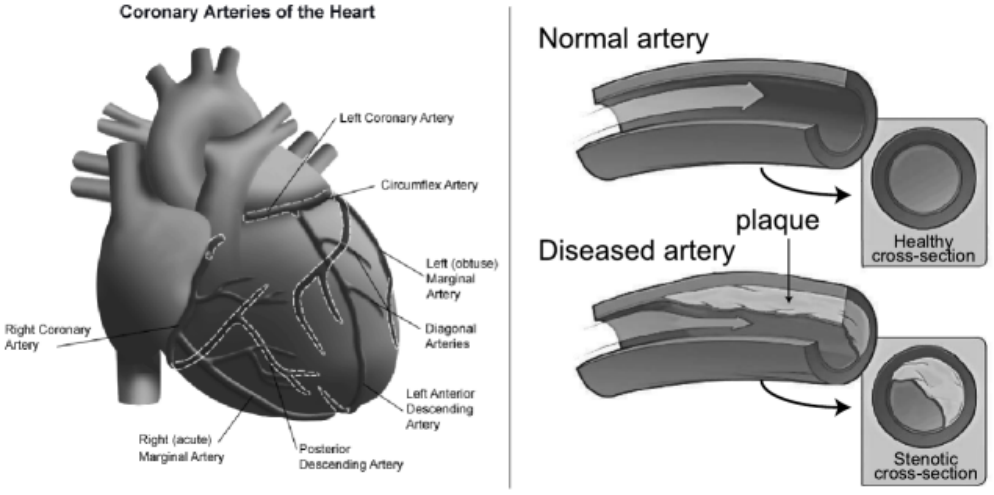

FIGURE 1.1: *Left*, heart and main coronary arteries anatomy (source: Jefferson University Hospitals). *Right*, schematic illustration of a vascular disease from (Schaap, 2010).

Commonly, CVDs are due to atherosclerosis characterized by the development and accumulation of plaques of different materials (i.e. cholesterol, calcium, fibro-fatty deposits) in artery walls reducing the blood flow. These plaques can be classified in three types: 1) non-calcified plaques, having a lower density compared with the vessel lumen, 2) calcified plaques, presenting high density scores, and 3) mixed plaques that have non-calcified and calcified elements within a single plaque (Pundziute et al., 2007).

1.1.2 Arteriography Vs. Computed Tomography Angiography

Conventional invasive coronary angiography (arteriography) is still the standard procedure to diagnose CVDs. This method consists in the insertion of a catheter in a principal artery (usually in the leg or the forearm) until it arrives near the zone to be captured. At this point, a contrast agent is injected into the vessel and the zone is imaged using X-ray based techniques. The result is a projected image (angiogram) of arterial trees in the region of interest, obtained with a high refreshment rate. Looking at these images, physicians can detect possible diseases because of the reduction of lumen and blood flow. However, this method is very invasive requiring a high expertise to avoid complications (damages to internal arteries, alterations in pulse, etc.), it requires a continuous flow of radiation and contrast agent injection, and sometimes the 2D projection hides narrowings that could be easily seen from another point of view.

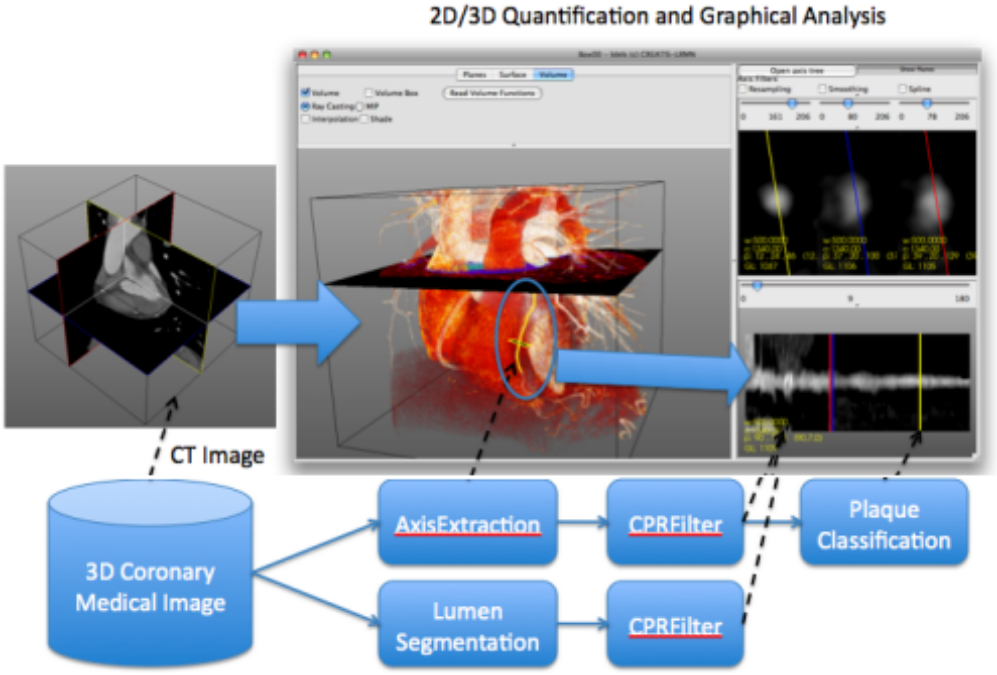

FIGURE 1.2: Left image presents 2D slices (axial, sagital, and coronal), center image is a volume rendering of the CTA, and right image presents CPR image with three orthogonal planes extracted at yellow, blue, and red locations.

Computed tomography angiography (CTA) is a non-invasive technique that consists of 3D acquisitions of the area of study, enhancing arteries by using a contrast medium. The high resolution of modern scanners (64-slice CT scanner can achieve a resolution of $0.3 \times 0.3 \times 0.4\,\mathrm{mm}^3$ per voxel) permits not only to make an approximation of the lumen volume, but also to locate and quantify soft and calcified plaques. Calcified lesions can be spotted as small, bright regions while soft plaques are usually lesions with lower intensity values than the artery lumen. The most common methods to study and visualize these images are multi-planar reformation (MPR), curved planar reformation (CPR), and 3D rendering techniques such as volume rendering or maximum intensity projections. Both MPR and CPR correspond to a set of 2D slices extracted from the original image: sagital, coronal, and axial views in the case of MPR, and a set of continuous slices, orthogonal to the axis tangent at each point, in the case of CPR (Figure 1.2 [1]). A more detailed revision about these techniques, their advantages and disadvantages can be found in (Wang, 2011).

Even if these new technologies improve the quality of the diagnosis and reduce the risks of invasive procedures, the amount of radiation used to obtain these images is considerably higher compared to the conventional methods. Moreover, the elevated quantity of data to evaluate due to 3D captures leads to other on-going challenges to detect clinically relevant problems.

1.2 Main Challenges and Workflow

Despite the possibility to improve the study of arteries thanks to high 3D resolution obtained by CTA, new difficulties appear from the image processing point of view. The following list proposed by Lesage (Lesage, 2009) summarizes the main problems in this research area:

- Size of data and resolution: CTA images typically reach sizes of $512 \times 512 \times 512$ voxels. In the case of coronaries, the radius varies between 1 to 10 voxels.
- Acquisition issues: noise, partial volume effect, and artifacts influence the results.
- Arteries complexity and variability: location, curvatures, sizes, and geometries are different in each patient.
- Pathologies and altering objects: presence of plaques, stents and bypasses affect the geometry and appearance.

[1] This visualization results make part of the creaCoro project (http://www.creatis.insa-lyon.fr/site/en/CreaCoro).

- Surrounding structures: in the case of coronary trees, vein networks and heart chambers can be mistaken for arteries because of their similar appearance or shape.

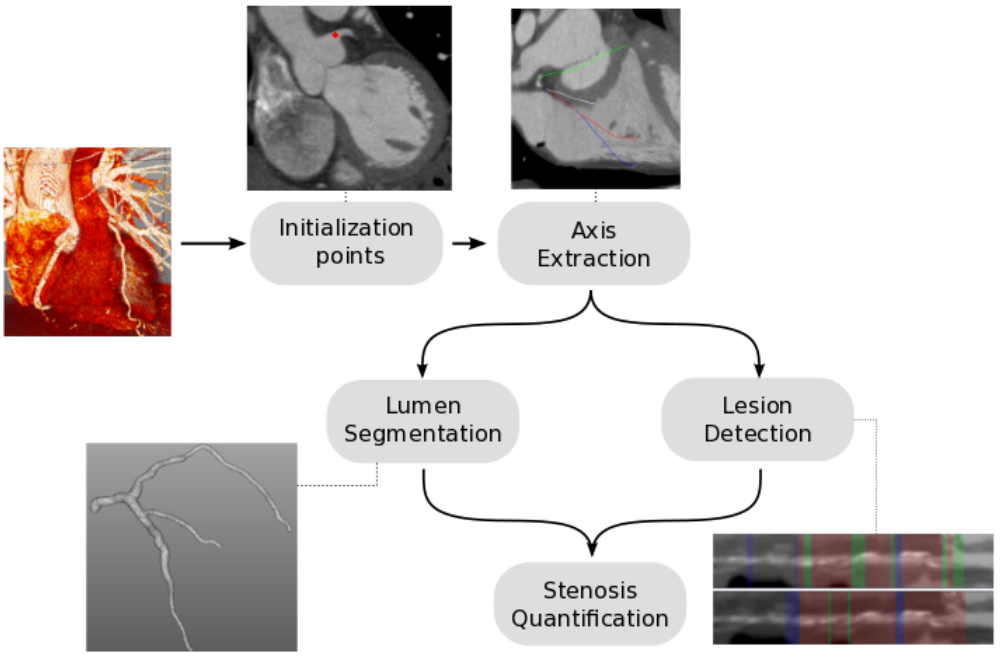

FIGURE 1.3: Workflow for coronary arteries analysis.

Considering these issues, the analysis of arteries and their pathologies is usually pursued by following a workflow that begins with the localization of some starting seed (generally at *ostia* locations) in order to initialize an axis extraction algorithm to identify the path of the main arteries. Additionally, the lumen segmentation can also be a result of this step or, depending on the approach used, it can give a first approach to the volume of interest to be processed. After these first steps, both lesion detection and stenosis quantification can be achieved in order to present specific and objective data about diseases to physicians (Figure 1.3).

1.3 Institutional Context

This project is involved in a scientific collaboration between CREATIS (Lyon, France) research laboratory and two universities in Bogota, Colombia: Universidad de los Andes and Universidad Javeriana. The three teams work together in a main project focused on the modeling of the coronary vascular tree in CTA + t images for lesions detection and stenosis quantification. This project is partly supported by the following institutions: Comité ECOS Nord (C11S01), Colciencias (1204-519-28996) and UniAndes Interfacultades (06-2010). Additionally, this thesis is the result of a recent agreement for a

Master's conjoint degree between the Universidad de los Andes (Bogota, Colombia) and Université Claude Bernard – Lyon 1 (Lyon, France).

Moreover, this study is partly motivated by the "Stenoses Detection, Quantification and Lumen Segmentation" challenge that will be held during the 15th International Conference on Medical Image Computing and Computer Assisted Intervention (MICCAI), Nice, France, 1-6 October 2012. This challenge makes part of an initiative[2] to create standard evaluation frameworks that permit research groups to explore, test, and compare their methods in standard datasets. Our group has participated and has obtained good results in the challenges held in 2008 for the coronary artery centerline extraction and the one in 2009 for the carotid lumen segmentation and lesions grading. Results of both challenges were already published and they are available online (Hameeteman et al., 2011, Schaap et al., 2009).

[2]Challenges objectives, rules, and results can be visited in http://www.grand-challenge.org.

Chapter 2

Related Work

2.1 General Overview

In image processing field and computer vision, segmentation consists in partitioning an image by means of the differences between an object of interest and the background. It is still considered a challenging task that depends on the image properties and its specific context. Vessel segmentation is mainly composed by the extraction of the vascular lumen which conserves a tubular shape (linear in 2D images) in normal cases and its an important step for posterior visualization techniques and pathology quantification. However, numerous complications appear caused by changes in vessels sizes and curvatures, inter- and intra-patient variability, proximity to similar surrounding structures, motion and acquisition artifacts, and presence of pathologies. Due to these difficulties, simple segmentation methods does not obtain an explicit and generic solution that covers the most part of the cases.

Many recent advanced studies has focused on this problematic, specially in coronary arteries (Schaap, 2010, Wang, 2011, Lesage, 2009, Zuluaga, 2011). Additionally, image processing challenges and reviews try to establish a general framework to compare methods and results obtained by different research groups. While some surveys presented classifications focusing on the algorithmic details, which do not facilitate the comparisons (Kirbas and Quek, 2004), a more recent survey in 3D vessel segmentation (Lesage et al., 2009) proposed a synthetic categorization based on three different criteria: 1) *a priori* knowledge about vessel geometry and appearance models, 2) definition and use of features that describe vascular lumen, and 3) schemes that have been proposed to perform lumen segmentation. The latter category can be roughly separated in two groups: 3a)algorithms requiring a previously extracted centerline (axis) and 3b) methods running in one pass (Schaap et al., 2011).

This chapter will be mainly focused on the most recent works in coronaries, specially the ones falling in the 3a group. Various axis extraction methods have been evaluated in (Metz et al., 2008) and demonstrated a high accuracy compared to reference axes. For this reason, even if it is still a hard task in terms of image processing, the results confirm the current feasibility of the assumption and the availability of a correct centerline for posterior processing tasks. In most of the cases, centerlines are also needed for posterior processing task such as stenosis detection and quantification.

2.2 Preprocessing

Some techniques require initial preprocessing steps not only for lumen segmentation, but also for axis extraction and stenosis detection. In order to enhance vessels and to have an starting point to segment, some functions have been proposed based on geometrical *a priori* and statistical regression methods.

One of the most common methods to enhance vessels was developed by Frangi et al. (1998) who proposed a multiscale method using a vesselness function based on Hessian matrix eigenanalysis. Despite of the good results of this method detecting tubular structures, it has elevated computational costs and presents problems in bifurcations and pathologies. Zhou et al. (2012) proposed changes in the Hessian-based vesselness function to obtain more accurate results and Zheng et al. (2011) defined a new learning-based vesselness function with better detection rates and faster computation. Other work preprocessed the image according to a prior knowledge of tissue densities expressed in Hounsfield Units (HU), e.g.: to focus on the arterial lumen, Lesage (2009) proposed to discard the densities beyond the range -24 HU to 576 HU, thus keeping voxels with a higher intensity than lung CT numbers and lower than calcifications. This is a simple method that can be useful to avoid the inclusion of calcified plaques, but can have different results depending on the acquisition, e.g.: make holes in lumen, or eliminate distal parts of the artery. A more image-dependent calculation of thresholding parameters is presented in (Tessmann et al., 2011) with the analysis of the centerline histogram.

Furthermore, some studies extend preprocessing to obtain an initial rough estimation of the vessel 3D geometry. This process helps to define a limited region to run more sophisticated algorithms reducing false positives and computational time. Carrillo et al. (2007) and Zhou et al. (2012) used spheres centered in the already extracted axis points with radii deduced from an estimate of the artery size. Linear (Xu et al., 2012) and non-linear approaches (Schaap et al., 2011, Kelm et al., 2011) have been also followed to approximate vessel diameters at a certain distance from the ostia. Another approach (Shahzad

et al., 2010) created a probability density field of coronary arteries based on registration of annotated CTA images.

2.3 Coronary Lumen Segmentation

Various solutions to vessel segmentation have been tested and reported in literature, from the most basic image processing techniques to the most advanced algorithms. One of the most classical approaches is region growing, which performs an iterative segmentation based on an inclusion criterion between some seed points (manually or automatically defined) and their vicinity. If neighboring voxels fulfill this condition, they are added as new seed points to continue the process. Bouraoui et al. (2008) detected ostia location to use them as seed points in a region-growing algorithm with a gray-level hit-or-miss transform as inclusion criteria. Renard and Yang (2008) and Tek et al. (2011) used points of a previously extracted axis as seed points to calculate thresholds and thus define the growing condition. The main drawback of region-growing is the difficulty to define an efficient stopping criterion and avoid leakages near to similar structures. Metz et al. (2007) proposed an additional restriction in order to avoid leakages by detecting a sudden large increase in the segmented volume.

Other restrictions can be set based on geometrical information and the adaptivity of the segmented mask into the vessel contours. Nain et al. (2004) exposed some preliminary results in CTA images of a segmentation method using an implicit deformable model with a soft shape prior, but no quantitative results were presented.

According to authors' validation tests and to the best of our knowledge, the two most accurate coronary segmentation methods respectively use a coarse-to-fine method with a robust combination of linear and non-linear regressions (Schaap et al., 2011), and a minimum average-cost path model that extracts vessel axis and estimates a vessel radius for each axis point (Zhu and Chung, 2011). However, the lack of standard validation data for coronary arteries segmentation increases the difficulty to compare the methods. Most of this work exposed qualitative results and some comparisons with the reference centerlines of MICCAI Challenge 2008, but just a few give information about overlap measures (e.g. Dice score) of segmented masks. The objective of the MICCAI Challenge 2012 is to bridge this gap.

Chapter 3

Materials and Methods

The methods of this study follow the conservative workflow that was presented in the introductory chapter. Main contributions were focused on the lumen segmentation step, but that required some additional work in the axis extraction methods and a review of the problematic in the subsequent lesion detection. In this chapter, I begin by presenting the materials used in the project, i.e. CTA images and reference data provided by the challenge organizers. Then, I continue talking about the axis extraction method developed in our group and an algorithm to center axes in the lumen. This first stage gives a base to test the segmentation methods that will be presented in the sequel of this chapter, and helps other developments to detect lesions that are being implemented in the group.

3.1 Materials

Datasets from MICCAI 2008 and 2012 challenges were used in this study. The first contest provided 32 CTA images from different machine vendors where eight of them are for training purposes and the rest for testing or validation steps. Training data has the reference centerlines of four main coronary arteries (RCA, LAD, LCX, and a left diagonal branch) and an estimated radius at each axis point. Figure 3.1 shows a 3D rendering of a mask constructed with information of estimated radius. The second challenge provides 48 datasets (18 for training) with a reference centerline extracted with three methods presented in MICCAI 2008 challenge. Complete annotations about plaques (plaque type, location and percentage of occlusion) are also given for each image. Voxel resolution in both sets was on average close to $0.3 \times 0.3 \times 0.4\,\mathrm{mm}^3$ and image dimensions of 512 x 512 x 400 voxels.

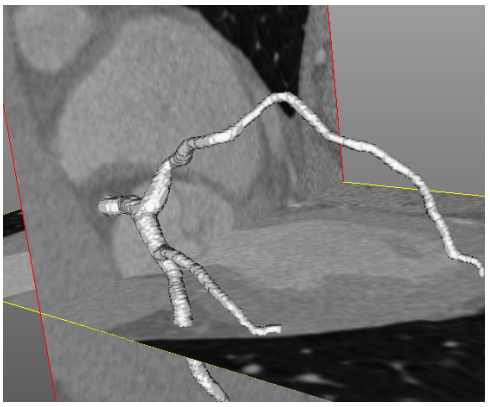

FIGURE 3.1: Surface rendering of a reference LCA tree.

3.2 Segmentation Assessment

The performance of a segmentation method is usually presented in terms to the similarity between the reference and the final result. Dice score makes this comparison based on the quantity of true positives (TP), true negatives (TN), false positives (FP), and false negatives (FN). According to these measures, Dice is defined as:

$$Dice = \frac{2VP}{(VP + FP) + (VP + FN)} \tag{3.1}$$

Other measures are usually used in order to calculate the percentage of well-classified points (accuracy), or to detect the capacity to obtain VP (sensitivity), or VN (specificity). These three methods are defined as follows:

$$Accuracy = \frac{VP + VN}{(VP + FP) + (VN + FN)} \tag{3.2}$$

$$Sensitivity = \frac{VP}{VP + FN} \tag{3.3}$$

$$Specificity = \frac{VN}{VN + FP} \tag{3.4}$$

Due to the difficulty to obtain a general framework to valid the methods in datasets from both challenges, these metrics were used in cases were a segmentation reference existed. However, a qualitative validation studying orthogonal planes to the centerline was used in the most of the cases, specially in methods with a high apparent accuracy.

3.3 Lumen Radius Estimation

Medical data confirms that coronary arteries radius in healthy cases fall in a range between 3 mm to 0.5 mm. Nevertheless, intra- and inter-patient shape variability and the presence of pathologies make difficult to estimate a generic mathematical function describing vessel at each point. For this reason, I analyzed the training data to evaluate a possible approximation of the change of lumen according to the distance from the ostium. Graphics of four datasets are shown in Section 4.2 (Fig. 4.2).

3.4 Axis Extraction

3.4.1 Tek-Dijkstra Extraction Method

Central axes are extracted using a strategy based on Dijkstra's algorithm to compute minimum spanning trees from graphs (Dijkstra, 1959). Such algorithm is useful in situations where data can be modeled as a graph, and minimum cost paths contain the solution of such problem. In the case of central axes extraction from CTA images, the graph is constructed from the image voxels (i.e. graph nodes or vertices) and by a medialness function associated to each image voxel. Such function should have small values (costs) near the center of vessels and large values elsewhere. Similar strategies have been used for quite a time in the literature, e.g.: Wink et al. (2002), Flórez Valencia et al. (2004).

The principal challenge in the use of the Dijkstra's algorithm resides in designing a good medialness function. In our case, we use the function proposed in (Gülsün and Tek, 2008), where the image gradient norm is analyzed along concentric rays in order to find the best radius that models the vessel as a cylinder.

Specifically, the algorithm we use starts with two user-given points; starting from these points, two minimum spanning tree is computed using the medialness function described before. The algorithm stops when both trees collide, thus extracting the central axis of the vessel. This semi-automatic method has been implemented by one of the members of our team. The resulting axis correctly follows the arterial pathway, but in some cross-sections it is not very well centered within the lumen.

3.4.2 Axis Correction

The main idea of an axis extraction method is to obtain the path (in terms of world coordinate points or voxel coordinates) that goes through the center of the lumen. This

precondition is essentially important to calculate measures or features that can be used to detect lesions, e.g. concentric rings (Zuluaga, 2011). However, even the reference axes provided by the challenge organizers are not always well centered, sometimes passing through plaques or close to the vessel wall (Figure 3.2). This is because manual tracing of the axes in 3D is a difficult task. Moreover, some automatic methods extract samples of the complete axis and an interpolation is performed to obtain the points in-between, which can also cause problems such as points located out of the vessel. Therefore, I propose a method to make a local correction of extracted centerline points, making the assumption that these points have higher intensity values compared to soft plaques and lower intensity than calcifications.

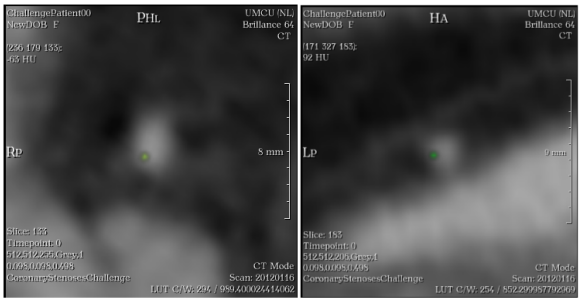

FIGURE 3.2: Examples of two non-centered slices. The green point represents the intersection between the reference axis and the cross-sectional plane.

First, the intensity histogram of the centerline is calculated and the corresponding CPR image is generated. Normally, intensity in vessel lumen decreases softly regarding the distance from the ostia, hence the histogram should be a tight uni-modal distribution. Outliers at minimum or maximum values or a bimodal distribution may be results of a centerline that go through soft plaques (lower intensity than lumen) and/or calcified plaques (higher intensity). Then, each orthogonal plane in the CPR image is processed with an adaptive thresholding method using as parameters the minimum and maximum values of the histogram. This step has as objective finding the region where the most lumen voxels are located and correct central point by slice. According to the lumen estimation explained in Section 3.3, leakages in lumen segmentation can be detected because the segmented area (calculated by using the estimated radius and assuming a circular area) exceeds the estimated area by a given factor. In that case, the lower threshold is incremented by one, until an acceptable lumen area is achieved. After this iterative process, the center of mass is calculated in the segmented region and it is assigned as the new central point in the slice. The complete process is summarized in Algorithm 1. This method could also be used to make a lumen segmentation, but the final result tends to underestimate the lumen by excluding voxels near the walls, so it will be not used for this purpose.

Algorithm 1 Centerline correction

Require: CPR image, axis points
  $hist \leftarrow histogram(axis)$
  $minThreshold \leftarrow min(hist)$
  $maxThreshold \leftarrow max(hist)$
  for $i = 0 \rightarrow$ number of planes **do**
    $estimatedArea \leftarrow estimateArea(i)$
    $segmentedArea \leftarrow thresholding(minThreshold, maxThreshold)$
    while $segmentedArea > estimatedArea$ **do**
      $minThreshold \leftarrow minThreshold + 1$
      $segmentedArea \leftarrow thresholding(minThreshold, maxThreshold)$
    end while
    $newCenter(i) \leftarrow computeCenterOfMass(segmentedArea)$
  end for

3.5 Coronary Lumen Segmentation

This section corresponds to the focus of my project. I have investigated both a "classical" approach using variants of region growing and active contour methods, and an approach based on classification and machine learning techniques.

3.5.1 Classical Approach

3.5.1.1 Local Region Growing

Region growing algorithms assume that the extracted region fulfills a criterion in all its points. However, establishing a global criterion in coronaries is difficult due to the changes in intensity and sizes, and the result can finish with big leakages or non-segmented sections. For this reason, our proposal bases on a local region growing approach limited by spheres and local statistic scores in enclosed axis points.

Using twice the value of the estimated radius in each centerline point, a sphere that locally encloses the artery is analysed. For this purpose, intensity average and standard deviation are calculated in artery centerline voxels inside the sphere. Some studies confirm that coronary lumen profiles in healthy cases follows a Gaussian-like distribution with higher intensities along the centerline and Gaussian attenuation toward the edges (Lesage et al., 2009). In an ideal Gaussian case, twice the value of the standard deviation around the average covers the 95% of whole distribution area. This factor was empirically adjusted using 1, 2, 2.5, and 3 times the standard deviation.

3.5.1.2 Variational Region Growing

Region growing methods are very frequently used due to their simplicity and possibility to make a fast extraction of a particular zone. However, the possibility to add more complex restrictions to achieve an optimal result is limited. Variational region growing (VRG) overcome these problems with the inclusion of an evolution equation that drives the segmentation to an optimal solution. Pacureanu et al. (2010) used VRG with an energy based on Frangi's vesselness function to detect lacuno-canalicular networks in bones. The method proposes the following derivative of this evolution function:

$$\Delta J\left(\phi^{n+1}\right) = \left(1 - 2\phi^{n}\right)\left[\Delta J_1\left(v\right) + \Delta J_2\left(f, v\right)\right] \tag{3.5}$$

$$\Delta J_1\left(v\right) = v\left[\left|v - \mu_{v_{in}}\right|^2 - \left|v - \mu_{v_{out}}\right|^2\right] \tag{3.6}$$

$$\Delta J_2\left(f, v\right) = \left(1 - v\right)\left[\left|f - \mu_{f_{in}}\right|^2 - \left|f - \mu_{f_{out}}\right|^2\right] \tag{3.7}$$

where f and v are the intensity and vesselness values ($0 \leq v \leq 1$) in the image, respectively; $\mu_{f_{in}}$, $\mu_{f_{out}}$, $\mu_{v_{in}}$, $\mu_{v_{out}}$ are the average of internal and external regions in both the original image and the vesselness measure. When a voxel is inside of a tubular structure, vesselness values are near to 1, so Equation 3.6 will be used. This means that information given by the vesselness measure is enough to describe a vessel. Conversely, when voxels are in the background, intensity values will be used (Equation 3.7) to enhance the results obtained by Frangi in discontinuities and bifurcations.

We tried to use the same approach in coronaries using both Frangi's (Frangi et al., 1998) and Sato's (Sato et al., 1998) vesselness measures due to the correspondence with the shape prior. This method depends on intensity averages of lumen and non-lumen voxels. Voxels located very far from the vessels of interest are likely to have characteristics that strongly differ from non-lumen voxels located near the vessels. For this reason, these tests were performed in VOIs defined by the union of the spheres defined in the previous subsection, to reduce the non-lumen region.

3.5.1.3 Active contours

Active contours is a powerful technique to delineate an object after the minimization of an energy associated with the contour. It does not correspond exactly to a segmentation

method, but it gives the contour(s) of the object to be segmented, thus a post-processing step is usually required. The accuracy and performance of active contours depend on the initialization curve, the selection of the energy function, and the optimization method to achieve a global minimum. The energy function is generally described as the sum of an internal energy associated with the elasticity and curvature of the contour, and an external energy that includes restrictions that can be extracted from the specific problem or the image properties, e.g. high gradients. Nonetheless, more advanced conditions can be used to achieve a good detection.

$$E = \oint_{C(s)} \frac{1}{1 + \|\nabla I\|} ds \tag{3.8}$$

$$E = \int_{x \in \Omega} (I - \mu)^2 dA + \int_{x \in \bar{\Omega}} (I - \bar{\mu})^2 dA \tag{3.9}$$

Lankton et al. (2007) proposed a hybrid functional energy that makes possible to integrate gradient constraints within a local optimum region. Geodesic active contours by Caselles et al. (1997) are used and it is classically presented as in the Equation 3.8. Similarly, region-based approaches are usually based in the minimization of the energy function defined by Chan and Vese (2001) in Equation 3.9. Taking both ideas, the suggested hybrid function is:

$$\oint_{C(s)} \int_{x \in \Omega} (I(x,s) - \mu_l(s))^2 + \int_{x \in \bar{\Omega}} (I(x,s) - \bar{\mu_l}(s))^2 ds, \tag{3.10}$$

where I corresponds to the intensity in the original image, and $\mu_l(s)$, $\bar{\mu_l}(s)$ are the intensity average in the internal region Ω and external region $\bar{\Omega}$, respectively.

This method starts by a simple curve, then it deforms contour based on statistics of interior and exterior regions until a convergence criterion is achieved. For our purpose, the method was tested in cross-sectional planes and the initial curves were small enough circles inside the lumen.

3.5.2 Classification Approaches

The following two methods were tested directly in the 3D space of the image. The main purpose of both approaches is to separate lumen voxels in one class, and non-lumen voxels in another one based on 3D image and geometrical features. In order to evaluate the performance of these methods, some statistical measures were used, e.g. Dice similarity score, accuracy, sensitivity, and specificity.

3.5.2.1 Geometric and Image Features

Machine learning approach avoids explicit modeling of the objects to be detected/segmented and aims at supervised or unsupervised training based on a set of features that are expected to characterize these objects and distinguish them from the remaining parts of the image. In order to learn the concept of arterial lumen, we selected a set of image and geometric features previously used in various vessel enhancement and vessel segmentation methods. This set was composed by intensity, gradient magnitude, and eigenvalues of the Hessian matrix, all of them calculated at eleven scales (using recursive Gaussian derivative filters) that correspond to the range of coronary radius. We start by the hypothesis that intensity is considerably elevated in lumen voxels, compared to their surroundings, and the gradient magnitude at the interior of the lumen should be low. Additionally, Hessian eigenvalues include information about shape according to the conditions expressed in table 3.1, where $|\lambda_1| \leq |\lambda_2| \leq |\lambda_3|$ (Frangi et al., 1998).

TABLE 3.1: Hessian eigenvalues values representing different structures.

Hessian eigenvalues	Structures
$\lambda_3 \approx \lambda_2 \ll \lambda_1 \approx 0$	tubular: vessels, bronchi
$\lambda_3 \approx \lambda_2 \approx \lambda_1 \ll 0$	bright blobs
$\lambda_3 \ll \lambda_2 \approx \lambda_1 \approx 0$	flat: bone boundaries, membranes

3.5.2.2 K-means Clustering

K-means clustering is one of the simplest and most commonly used semi-supervised algorithms. It starts with a initial partition defined by the centroids of each cluster and reassigns clusters based on the similarity between each data sample and the centers until a convergence criterion is met. The most popular metric to compute similarity is the Euclidean distance. In this case, K-means (k=2) is used to detect classes of lumen and non-lumen voxels in each sphere, in the same way of the local region growing method sphere method. The features used for this purpose were: minimum distance from a voxel to the centerline, Hessian eigenvalues, and intensity at different scales.

3.5.2.3 Support Vector Machines

In this section, we explore a different approach with an automatic segmentation defined as a problem of supervised classification using Support Vector Machines (SVM). SVM is commonly used in classification and regression tasks and it is well known due to its capacities to achieve good generalization and maintaining the maximum possible margin

between classes. This is made by the use of a kernel function that projects data into high-dimensional spaces where the class separability is possible.

Training and validation data for lumen segmentation was obtained from MICCAI 2008 challenge. The measures were obtained at each voxel in a restricted VOI defined by twice the radius given by organizers. For training data we assure that the machine has enough information about lumen and non-lumen classes to learn both concepts and their possible variations. According to recommendations given by Chang and Lin (2011), we use a radial basis function as kernel and optimization is achieved by a grid-search on the kernel parameter γ and the regularization term C.

Chapter 4

Results

4.1 Axis Correction

At the beginning of this work, axis given by organizers were used to study the given coronary arteries. However, CPR images created with those axes showed that some slices were not centered in the vessel lumen, as in the example displayed before in Figure 3.2. Due to the importance of this precondition in the following methods, our axis extraction technique was used and it achieved a better centering closer to the expected center of the lumen. Nevertheless, the problem persisted in some of the cases and recentering was required.

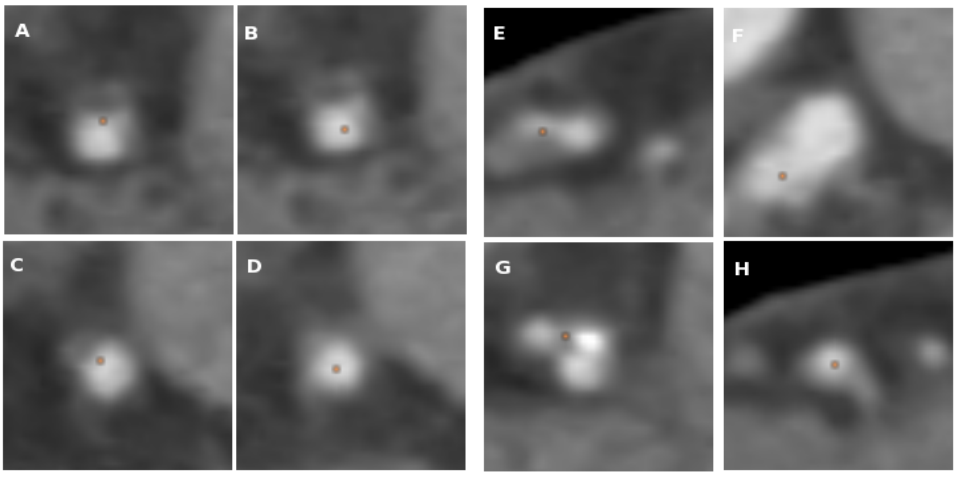

FIGURE 4.1: The four slices in the left present the comparison between axis before correction (A, C) and after correction (B, D). Images on the right present wrong correction in bifurcations (E,F), calcified plaques (G), and the result in a distal zone with a little bifurcation (H).

Recentering showed good results in healthy slices, in both proximal and distal zones (Figure 4.1). However, the current condition to define the new center as the centroid of

the lumen voxels often fails at bifurcations. As long as the branches are connected in a cross-sectional image and the total region size is under the maximum area threshold, the centroid tends to fall in-between the branches instead of being centered within one of them. The same situation occurs when weakly contrasted calcified plaques are included in the segmentation. Generally, these specific problems tend to set centers in plaques or outside the artery.

4.2 Lumen Radius Estimation

Training data gives some information about the lumen radius variation according to the distance from the ostia. Plotting main arteries by dataset shows high variations of radius due to possible plaques that reduce artery lumen (Figure 4.2). Nevertheless, in the most of the cases a soft monotonous decreasing behavior applies and could be approximated by a constant decreasing factor. For this reason, the average of the linear regressions describes the general behavior of the coronary arteries. In the case presented, the regression was expressed by the equation: $y = 0.01x + 2.49$ in mm. Additionally, the methods evaluated require generally an estimation that encloses the artery. Using the result of this study, it is sufficient to use a linear approximation of radius values with the prior knowledge that coronary arteries won't be thicker than 4 mm in the ostia and 1 mm at 200 mm from the ostia. This was very recently confirmed by Xu et al. (2012) who made the same linear approximation for the diameter estimation.

4.3 Classical Approaches

All the tested methods have shown some advantages, as well as problems specially in distal zones and lesion locations. Even if all these techniques achieve a partial segmentation of lumen, not all of them are suitable or exploitable due to elevated computation times and dependence on many parameters.

Results for local adaptive region growing technique show good results for healthy cases. Fifteen arteries were evaluated using this method (using the mean $\pm$ 3 times the standard deviation as stopping criterion) and the results can be divided into three categories: acceptable (9), poor (4), and bad (2) segmentation. Examples of these results are presented in Figure 4.3.

The problems appear specially in distal zones and regions with lesions. In most of the cases this problem is caused by axis not centered in the vessel lumen causing the inclusion of voxels with very different intensity values in each sphere, thus the standard deviation

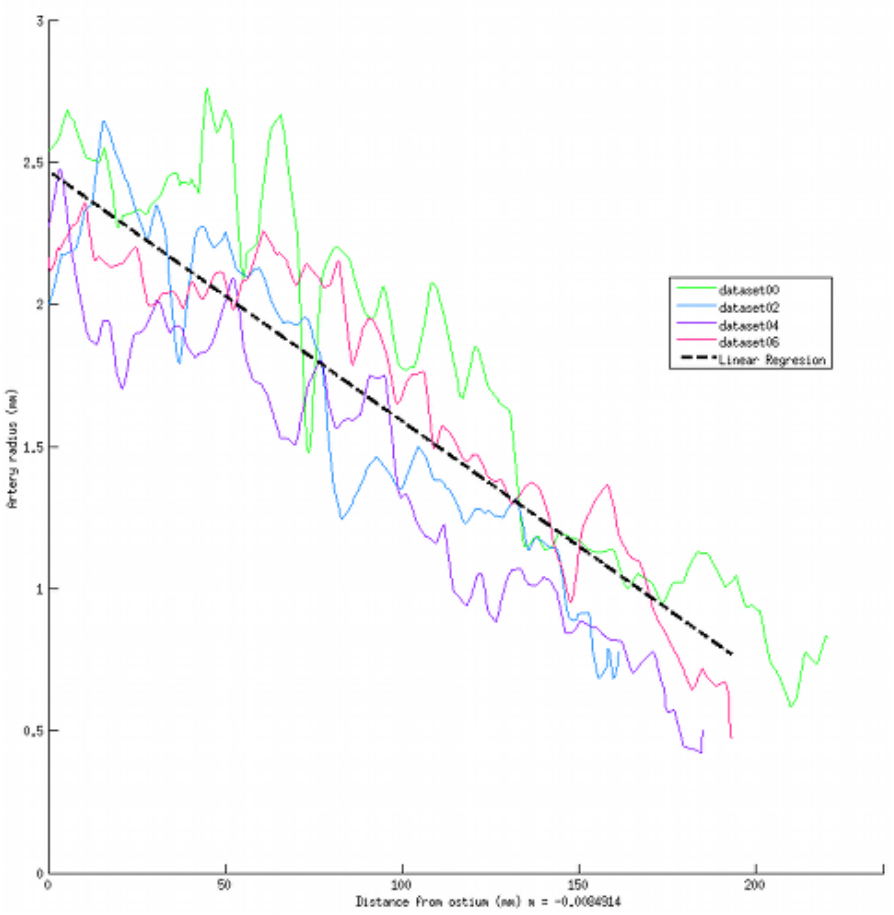

FIGURE 4.2: Variation of radius (mm) according to the distance (mm) in RCA over 4 datasets of MICCAI 2008 challenge.

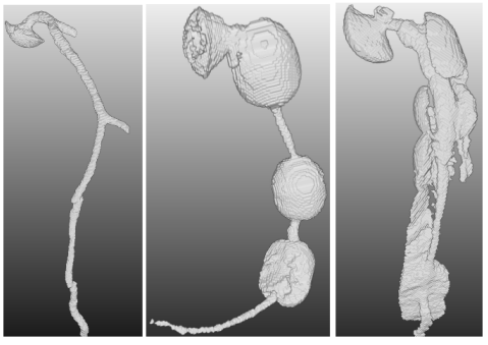

FIGURE 4.3: *Left*, an acceptable segmented artery that includes also detected bifurcations. *Center*, a poor result with local leakages enclosing plaques. *Right*, a bad result over all the artery, mainly caused by non-centered axis.

is considerably high reducing lower threshold (soft plaques included) and increasing the higher threshold in the region-growing inclusion criteria. This happens also in distal artery zone where lumen intensities are similar to background intensities. Additional restrictions to avoid leakages as the one used in axis correction could improve results in wrong cases.

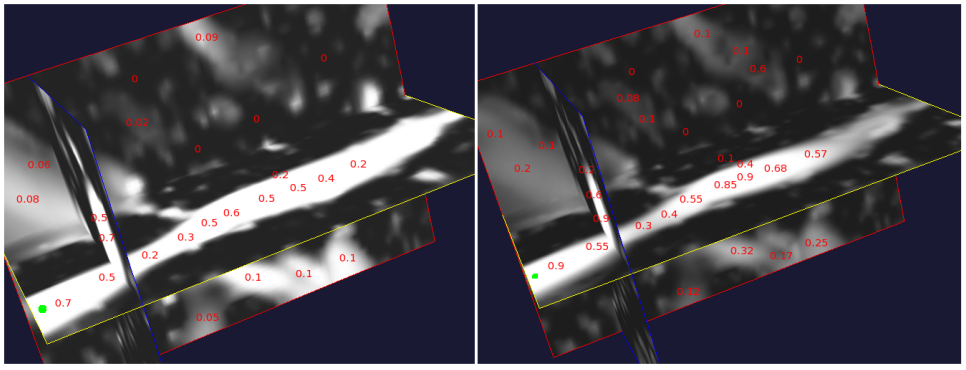

FIGURE 4.4: *Left*, Frangi response. *Right*, Sato response.

VRG adds geometrical constraints to achieve a good segmentation using a seed that in this case is located in an ostium. However, as a region-based approach, it depends on the correct definition of the external and internal areas to calculate statistical values. To evaluate the accuracy in regions, the method was tested in proximal and distal artery zones using Frangi's and Sato's vesselness functions. The constant parameters that require both functions were set as previous authors recommendations (for Frangi, $a = 0.5$, $b = 0.5$, and $c = 400$; for Sato, $a = 0.5$, $b = 0.5$). A depiction of both vesselness values in a proximal zone of the artery is presented in Figure 4.4.

A recurrent problem in this and the following tests when comparing with reference data of the challenge is the inclusion of some lumen voxels, such as in bifurcations, that don't exist in the validation mask. These cases should be considered as true positives because they are inside the lumen, but similarity and statistical measures will always include them as errors in the segmentation. A clear example of this situation is presented in the proximal region where the Dice value of VRG using Sato measure was 79.98%. Nevertheless, the 3D rendering of the result (Figure 4.5) confirms that the score could be higher if the bifurcation had been included as lumen.

Despite the good results of the proximal segmentation, distal regions presented a different behavior, even changing the vesselness function. After these results, the method was tested in a complete artery using two different VOIs to limit the quantity of non-lumen voxels: 1) a VOI produced with twice the reference radius, 2) a cylinder with a constant radius big enough (6.36mm radius) to enclose the artery at all the points (Figure 4.6). The tests show that the method is not well adjusted for this segmentation task. In this

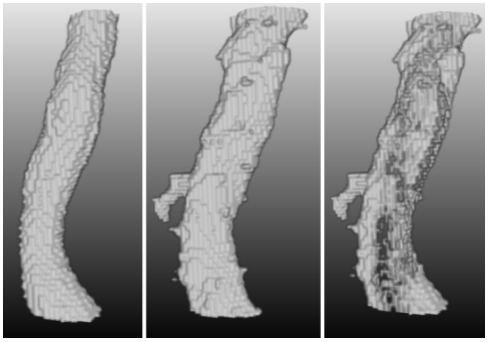

FIGURE 4.5: *Left*, reference mask. *Center*, VRG result using Sato vesselness. *Right*, XOR between both binary masks. Reference mask doesn't include lumen voxels that may appear in segmentation methods.

case (that is considered as a simple one), processing take a considerable amount of time and it doesn't achieve better results than the ones obtained by a simple thresholding.

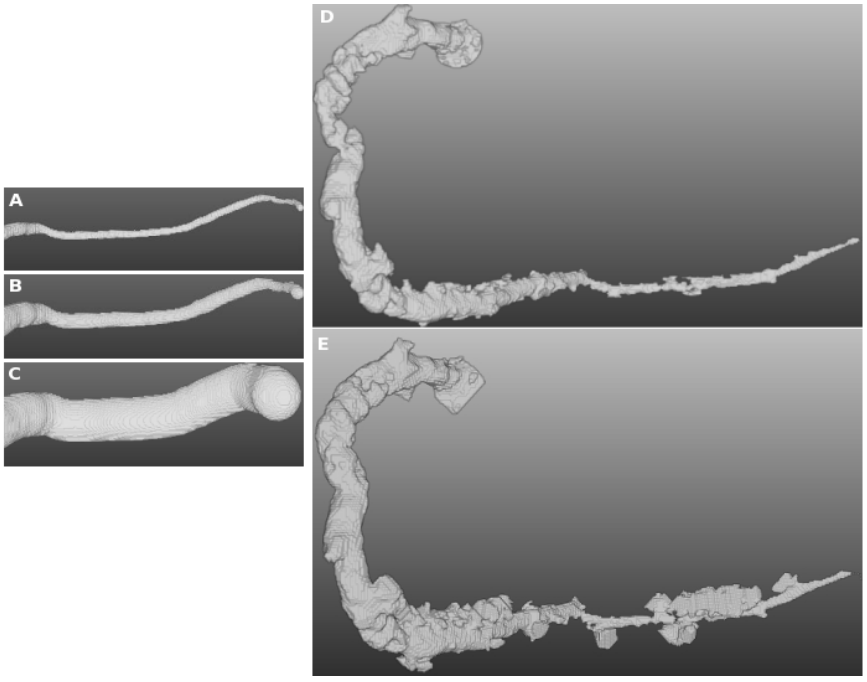

FIGURE 4.6: A, B and C respectively correspond to the reference mask, a VOI with twice the radius of the reference, and a VOI with a large constant radius. Results using VRG with Frangi's vesselness within B and C are presented in D and E respectively.

Finally, one of the best segmentation results was obtained with the active contours approach that use a region- and gradient-based energy function. This method was tested in the 2D planes of the CPR image, so the lumen detection was based on the detection of high contrasts between lumen and background or plaques. The algorithm implementation in Matlab was obtained from the website of the authors (Lankton et al., 2007). It receives as parameters the initial contour (a little region in the center of the lumen), a smoothness parameter (0.2), and the maximum number of iterations (120),

all of them were set empirically. A good result in a calcified orthogonal slice is presented in Figure 4.7.

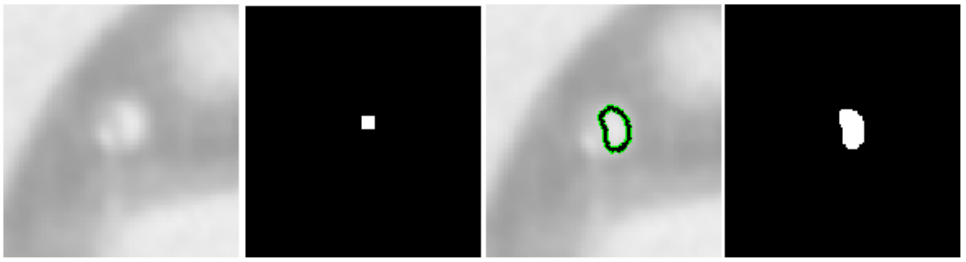

FIGURE 4.7: From left to right, orthogonal slice from the original image, initial contour, deformed contour after 100 iterations, and final segmentation.

Despite its good qualitative results over all the artery (no leakages due to curvature restrictions), slices with soft plaques or smooth calcified plaques that have not a good contrast with lumen, are missed or finish in a subsegment. A few cases showed a sub-segmented result near to calcifications, probably caused by a local minimum when the contour touches the calcification and the vessel wall. Some additional examples are presented in Figure 4.8. Also, some complications were seen in considerably big bifurcations where the active contour didn't increase its radius but it collapsed into the central point.

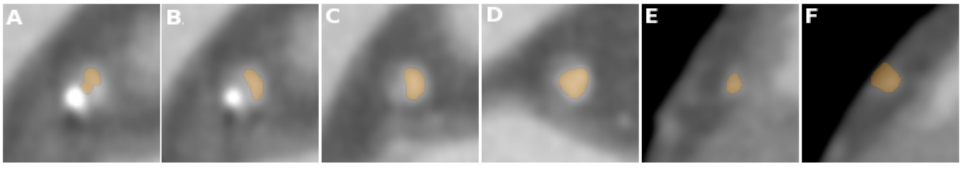

FIGURE 4.8: All the slices have its correspondent segmentation overlaid in orange. A and B are slices in calcified plaques, the first one presents a sub-segmentation, the second is correct. C avoids a soft plaque. D includes a little calcification with smooth contrast. E and F are the results obtained in distal slices.

4.4 Classification Approaches

The last two methods follow a different approach that tries to describe two classes: lumen and non-lumen. The features described in the Methods section were used for this purpose. In the case of k-means clustering ($k = 2$), a subset of those features was used according to an evaluation made by visualizing the sparseness of data created by the selected features. The conclusions of that revision showed that the two highest Hessian eigenvalues give more information about vessel lumen, compared to the values assigned to the background. The set made by these features and the intensity calculated at 3 scales (1.5, 2.0 and 3.0 mm) expanded by the additional feature of Euclidean distance from a voxel to the axis centerline, were the base of the k-means classification within spheres.

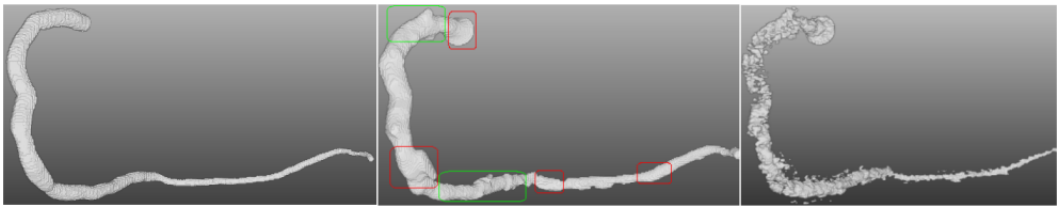

FIGURE 4.9: *Left*, reference segmentation. *Center*, k-means clustering result. Green areas correspond to correct results that do not appear in reference. Red means errors that increase false positives rate. No color, means a good segmentation but some generally overpass the lumen. *Right*, thresholding result.

As it was presented in the classical approaches, statistical measures can have an erroneous response because reference masks do not include all the lumen information. K-means clustering presented a Dice score of 66.48% that is apparently slightly better than a thresholding technique (65.20%). Nevertheless, looking in detail at the results of the segmentation (Figure 4.9), lumen portions that do not appear in reference mask were marked as errors. The problem of this method is the initialization of cluster centroids, specially for non-lumen class. This centroid was calculated at the border of the sphere assuming that non-lumen voxels were present, but that drives to the second problem: the number of classes in the sphere could be more than two, specially in plaque locations and near the lungs in the distal part of the arteries.

TABLE 4.1: Variation of parameters C and γ for SVM training.

Parameter	Values
C	$2^{-3}, 2^{-1}, 2^{3}, 2^{5}, 2^{7}$
γ	$2^{-10}, 2^{-7}, 2^{-5}, 2^{-3}, 2^{-1}$

The second test with classification techniques was using SVM following a supervised approach. Reference data from different coronary arteries was used to extract lumen training and testing data, and some manually selected regions in non-lumen tissues conformed data for the non-lumen class. Some tests were previously conducted in carotid arteries taking 650.000 samples to train and 1'500.000 to validate and test the method. The grid-search for SVM optimum parameters was performed using the training dataset and the values in Table 4.1. Best performance was found with $\gamma = 2^{-5}$ and $C = 2^{-3}$.

In the coronary arteries study, a considerable quantity of lumen data (96.987 samples) was randomly selected from the reference masks of the 3 main arteries (RCA, LAD, LCX). Conversely, non-lumen data (596.610 samples) was extracted from the region between reference vessel surface and the cylindrical VOI wall. However, samples with less than 5 voxels of distance from the vessel were removed to avoid confusions between lumen and non-lumen classes. This precondition is also used in (Zheng et al., 2011).

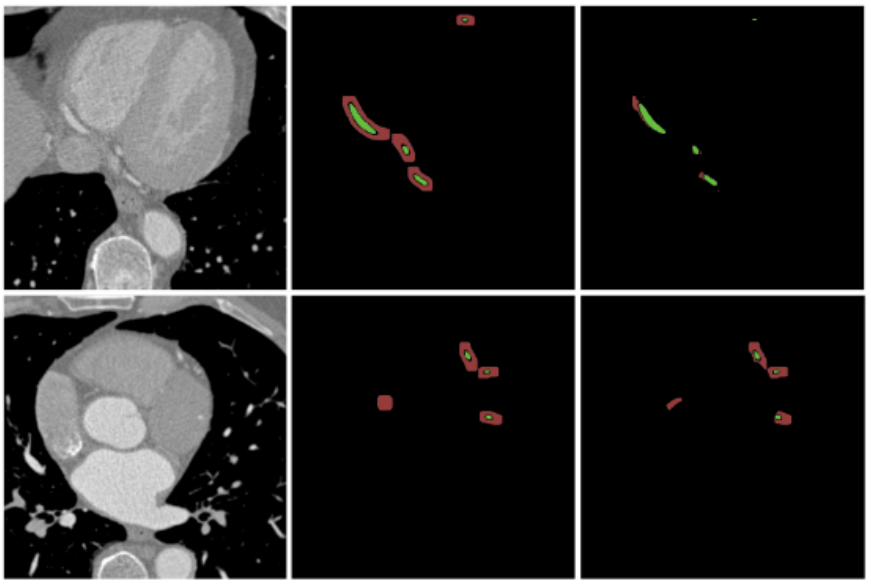

FIGURE 4.10: *Left*, axial slices in the original image. *Center*, labeled test data (non-lumen voxels in red, lumen in green). *Right*, segmentation using SVM produces many false positives (in red).

The obtained partial results were very poor and discouraging, compared to the other techniques. The best Dice similarity score was close to 45%. Sensitivity and specificity scores were higher (over 60%) because of the unbalanced quantity of data for each class. This is a big problem in this segmentation approach because the quantity of lumen data is considerably lower compared to the high number of different non-lumen voxels. Figure 4.10 presents one example of a SVM segmentation using the best selected parameters. Generally, the technique reduces the number of non-lumen voxels, but many false positive samples remain in the final segmentation.

Chapter 5

Conclusions

This work exposed six methods to achieve the coronary lumen segmentation in CTA images. Additionally, it presented a method for centerline extraction and an algorithm to recenter these axes. These two steps are considered essential to perform a correct analysis in coronary arteries and for an accurate lesion detection.

According to these needs, our study showed that existing axis extraction methods and challenge reference data can have erroneous axis points, specially when the centerline goes through plaques or passes very close to the vessel wall. The recentering process helped to correct some of these problems, but it was sensitive to bifurcations and calcified plaques. Nevertheless, this information could be used for an initial detection of these cases that affect segmentation (e.g. selecting seeds for region-growing and clustering schemes), and lesion detection results (e.g. calculation of 2D concentric features). Additionally, a centerline located in the arterial lumen helps to understand the variation of lumen intensity due to attenuation of the contrast-medium. Prior knowledge about lumen intensity should be helpful to adjust parameters for each patient, reducing problems due to inter-patient variability. For example, it was expected that lumen intensities fall when increasing the distance from the ostium, but some cases were found where lumen intensity increased in the middle of the artery, even with higher values than calcified plaques. A similar situation happens with lumen radius that can have sudden increase in distal regions. All these particularities confirm that the explicit modeling of coronary arteries and intensity profiles is a very challenging task, requiring the combination of different methods to include most of the possible variations of the problem.

All the six tested segmentation methods had some advantages and disadvantages. In our tests, region growing, active contours, and clustering techniques had good results in healthy vessels. Additionally, the possibility to introduce shape restrictions (such as in VRG or active contours) should increase accuracy, reduce leakages, and avoid

problems in bifurcations. However, including lesions in segmented regions is a common problem that need more information about context and continuity in the segmentation. Additionally, the solutions proposed in order to learn and describe an explicit model obtained poor results, specially for SVM. This can be possibly explained by three main problems: redundancy in the reference data caused by bad reference segmentations, the features selected to describe a vessel were not the correct, and selected lumen and non-lumen data was not enough to cover all the cases in a voxel-by-voxel approach. However, further tests are needed in order to find a correct feature set to describe the problem and define a complete training and validation framework to avoid inconsistencies.

Moreover, standard validation data for coronary vessel analysis is required in order to make an objective comparison of methods. Some synthetic frameworks would be useful, however it is difficult to cover all the healthy and non-healthy cases, besides the difficulty of modeling geometrical and anatomical conditions (heart cavities, myocardium, lungs, vessel trees). Nevertheless, an integrated framework to work and to test methods with the same images would be highly desirable. Generally, radiologist's diagnosis is not based only in the information given in the 2D orthogonal plane at a certain distance. They also need to evaluate previous and posterior slices to understand changes in lumen intensity and radius in a particular region. This kind of context knowledge should be included (using automatic or interactive alternatives) in coronaries study in order to make accurate estimations and confirm good or bad segmentations. These conditions should be also added in learning processes, such as in classification methods. Future work will be focused on visualization cues to help the analysis of coronary arteries and the extraction of quantitative scores taking advantage of the best results obtained in this experience towards the lesion detection and stenosis quantification.

References

World Health Organization. Global status report on noncommunicable diseases 2010. Technical report, World Health Organization, 2011.

M. F. Di Carli and R. Hachamovitch. New technology for noninvasive evaluation of coronary artery disease. *Circulation*, 115(11):1464–1480, 2007. doi: 10.1161/CIRCULATIONAHA.106.629808.

Christina Biermann, Ilias Tsiflikas, Christoph Thomas, Bernadette Kasperek, Martin Heuschmid, and Claus Claussen. Evaluation of computer-assisted quantification of carotid artery stenosis. *Journal of Digital Imaging*, 25:250–257, 2012. ISSN 0897-1889. doi: 10.1007/s10278-011-9413-y.

M. Schaap. *Quantitative Image Analysis in Cardiac CT Angiography.* PhD thesis, Erasmus University Rotterdam, 2010.

G. Pundziute, J.D. Schuijf, J.W. Jukema, E. Boersma, A.J.H.A. Scholte, L.J.M. Kroft, E.E. van der Wall, and J.J. Bax. Noninvasive assessment of plaque characteristics with multislice computed tomography coronary angiography in symptomatic diabetic patients. *Diabetes Care*, 30(5):1113–1119, 2007.

Chunliang Wang. *Computer-Assisted Coronary CT Angiography Analysis: From Software Development to Clinical Application.* PhD thesis, Linköping University, Radiology, Center for Medical Image Science and Visualization, CMIV, Faculty of Health Sciences, 2011.

David Lesage. *Modèles, primitives et méthodes de suivi pour la segmentation vasculaire. Application aux coronaires en imagerie tomodensitométrique 3D.* PhD thesis, Télécom ParisTech, 2009.

K. Hameeteman, M.A. Zuluaga, M. Freiman, L. Joskowicz, O. Cuisenaire, L. Flrez Valencia, M.A. Glsn, K. Krissian, J. Mille, W.C.K. Wong, M. Orkisz, H. Tek, M. Herndez Hoyos, F. Benmansour, A.C.S. Chung, S. Rozie, M. van Gils, L. van den Borne, J. Sosna, P. Berman, N. Cohen, P.C. Douek, I. Snchez, M. Aissat, M. Schaap, C.T.

Metz, G.P. Krestin, A. van der Lugt, W.J. Niessen, and T. van Walsum. Evaluation framework for carotid bifurcation lumen segmentation and stenosis grading. *Medical Image Analysis*, 15(4):477 – 488, 2011. ISSN 1361-8415. doi: 10.1016/j.media.2011.02.004.

M. Schaap, C. T. Metz, T. van Walsum, A. G. van der Giessen, A. C. Weustink, N. R. Mollet, C. Bauer, H. Bogunović, C. Castro, X. Deng, E. Dikici, T. O'Donnell, M. Frenay, O. Friman, M. Hernández Hoyos, P. H. Kitslaar, K. Krissian, C. Kühnel, M. A. Luengo-Oroz, M. Orkisz, Ö. Smedby, M. Styner, A. Szymczak, H. Tek, C. Wang, S. K. Warfield, Y. Zhang, S. Zambal, G. P. Krestin, and W. J. Niessen. Standardized evaluation methodology and reference database for evaluating coronary artery centerline extraction algorithms. *Medical Image Analysis*, 13(5):701 – 714, 2009. ISSN 1361-8415. doi: DOI:10.1016/j.media.2009.06.003.

Maria Alejandra Zuluaga. *Methods for automation of vascular lesions detection in computed tomography images*. PhD thesis, Université Claude Bernard Lyon 1, France and Universidad de los Andes, Bogota, Colombia, 2011.

C. Kirbas and F. Quek. A review of vessel extraction techniques and algorithms. *ACM Computing Surveys*, 36(2):81–121, June 2004.

David Lesage, Elsa D. Angelini, Isabelle Bloch, and Gareth Funka-Lea. A review of 3D vessel lumen segmentation techniques: Models, features and extraction schemes. *Medical Image Analysis*, 13(1):819–845, 2009. doi: 10.1016/j.media.2009.07.011.

M. Schaap, T. van Walsum, L. Neefjes, C. Metz, E. Capuano, M. de Bruijne, and W. Niessen. Robust shape regression for supervised vessel segmentation and its application to coronary segmentation in CTA. *IEEE Transactions on Medical Imaging*, 30(11):1974 –1986, nov. 2011. ISSN 0278-0062. doi: 10.1109/TMI.2011.2160556.

C Metz, M Schaap, T Van Walsum, A Van Der Giessen, A Weustink, N Mollet, G Krestin, and W Niessen. 3D Segmentation in the Clinic: A Grand Challenge II – Coronary Artery Tracking. In *Medical Image Computing and ComputerAssisted Intervention – MICCAI*, Brisbane, Australia, 2008.

A. F. Frangi, R.F. Frangi, W.J. Niessen, K.L. Vincken, and M.A. Viergever. Multiscale vessel enhancement filtering. pages 130–137. Springer-Verlag, 1998.

C. Zhou, H. P. Chan, A. Chughtai, S. Patel, L. M. Hadjiiski, J. Wei, and E. A. Kazerooni. Automated coronary artery tree extraction in coronary ct angiography using a multiscale enhancement and dynamic balloon tracking (MSCAR-DBT) method. *Computerized Medical Imaging and Graphics*, 36(1):1 – 10, 2012. ISSN 0895-6111. doi: 10.1016/j.compmedimag.2011.04.001.

Y. Zheng, M. Loziczonek, B. Georgescu, S.K. Zhou, F. Vega-Higuera, and D. Comaniciu. Machine learning based vesselness measurement for coronary artery segmentation in cardiac ct volumes. In Benoit M. Dawant and David R. Haynor, editors, *SPIE Medical Imaging*, volume 7962, page 79621K, Lake Buena Vista, Florida, USA, 2011. doi: 10.1117/12.877233.

M. Tessmann, F. Vega Higuera, B. Bischoff, Jörg Hausleiter, and Günther Greiner. Automatic detection and quantification of coronary calcium on 3D CT angiography data. *Computer Science*, 26(1-2):117–124, 2011.

J. F. Carrillo, M. Hernández Hoyos, E. E. Dávila-Serrano, and M. Orkisz. Recursive tracking of vascular tree axes in 3d medical images. *Int J Comput Assisted Radiol Surg*, 1(6):331–339, 2007. doi: 10.1007/s11548-007-0068-6.

Y. Xu, G. Liang, G. Hu, Y. Yang, J. Geng, and P.K. Saha. Quantification of coronary arterial stenoses in CTA using fuzzy distance transform. *Comp. Med. Imag. and Graph.*, 36(1):11–24, 2012.

B.M. Kelm, S. Mittal, Y. Zheng, A. Tsymbal, D. Bernhardt, F. Vega Higuera, S.K. Zhou, P. Meer, and D. Comaniciu. Detection, grading and classification of coronary stenoses in computed tomography angiography. In *Medical Image Computing and Computer-Assisted Intervention – MICCAI*, volume LNCS 6893, Part III, pages 25–32, Toronto, Canada, 2011.

R. Shahzad, M. Schaap, T. van Walsum, S. Klien, A. C. Weustink, L. J. van Vliet, and W. J. Niessen. A patient-specific coronary density estimate. In *IEEE International Symposium on Biomedical Imaging: from Nano to Macro*, ISBI'10, pages 9–12, Piscataway, NJ, USA, 2010. IEEE Press. ISBN 978-1-4244-4125-9.

B. Bouraoui, C. Ronse, J. Baruthio, N. Passat, and Ph. Germain. Fully automatic 3d segmentation of coronary arteries based on mathematical morphology. In *IEEE International Symposium on Biomedical Imaging: from Nano to Macro*, ISBI'08, pages 1059–1062, Paris, France, 2008. IEEE Press.

F. Renard and Yongyi Yang. Image analysis for detection of coronary artery soft plaques in MDCT images. In *IEEE International Symposium on Biomedical Imaging: from Nano to Macro*, ISBI'08, pages 25–28, Paris, France, 2008. IEEE Press. doi: 10.1109/ISBI.2008.4540923.

H. Tek, Y. Zheng, M. A. Gulsun, and G. Funka-Lea. An automatic system for segmenting coronary arteries from CTA. In *MICCAI Workshop on Computing and Visualization for Intravascular Imaging*, pages 47–54, Toronto, Canada, 2011.

C. Metz, M. Schaap, A. van der Giessen, T. van Walsum, and W. Niessen. Semi-automatic coronary artery centerline extraction in computed tomography data. In *IEEE International Symposium on Biomedical Imaging: from Nano to Macro*, ISBI'07, pages 856–859, Washington, DC, USA, 2007. IEEE Press. doi: 10.1109/ISBI.2007.356987.

D. Nain, A.J. Yezzi, and G. Turk. Vessel segmentation using a shape driven flow. In *Medical Imaging Computing and Computer-Assisted Intervention – MICCAI*, volume LNCS 3216, pages 51–59, St Malo, France, 2004. doi: 10.1007/978-3-540-30135-6_7.

N. Zhu and A. Chung. Minimum average-cost path for real time 3d coronary artery segmentation of CT images. In Gabor Fichtinger, Anne Martel, and Terry Peters, editors, *Medical Image Computing and Computer-Assisted Intervention MICCAI 2011*, volume LNCS 6893 of *Lecture Notes in Computer Science*, pages 436–444, Toronto, Canada, 2011. Springer Berlin / Heidelberg. ISBN 978-3-642-23625-9. doi: 10.1007/978-3-642-23626-6_54.

E. W. Dijkstra. A note on two problems in connexion with graphs. *Numerische Mathematik*, 1(1):269–271, 1959. doi: 10.1007/BF01386390.

Onno Wink, Ro F. Frangi, Bert Verdonck, Max A. Viergever, and Wiro J. Niessen. 3d mra coronary axis determination using a minimum cost approach. In *Magnetic Resonance in Medicine*, pages 1169–1175, 2002.

L. Flórez Valencia, F. Vincent, and M. Orkisz. Fast 3d pre-segmentation of arteries in computed tomography angiograms. In *Int Conf Comput Vision Graphics*, volume 32, pages 361–366, Warsaw, Poland, 2004. Springer Verlag, Publ., Springer Verlag, Publ. doi: 10.1007/1-4020-4179-9_52.

M. A. Gülsün and H. Tek. Robust vessel tree modeling. In *Medical Image Computing and Computer-Assisted Intervention*, MICCAI '08, pages 602–611, Berlin, Heidelberg, 2008. Springer-Verlag. ISBN 978-3-540-85987-1. doi: 10.1007/978-3-540-85988-8_72.

A. Pacureanu, C. Revol-Muller, J.L. Rose, M. Sanchez-Ruiz, and F. Peyrin. A vesselness-guided variational segmentation of cellular networks from 3D Micro-CT. In *IEEE International Symposium on Biomedical Imaging: from Nano to Macro*, pages 912 – 915, Rotterdam, Netherlands, 06/2010 2010. doi: 10.1109/ISBI.2010.5490135.

Y Sato, S. Nakajima, Nobuyuki Shiraga, Hideki Atsumi, Shigeyuki Yoshida, Thomas Koller, Guido Gerig, and Ron Kikinis. Three-dimensional multi-scale line filter for segmentation and visualization of curvilinear structures in medical images. *Medical Image Analysis*, 2(2):143 – 168, 1998. ISSN 1361-8415. doi: 10.1016/S1361-8415(98)80009-1.

S. Lankton, S. Nain, A. Yezzi, and A. Tannenbaum. Hybrid geodesic region-based curve evolutions for image segmentation. In *SPIE Medical Imaging*, volume 6510, page 65104, 2007.

V. Caselles, R. Kimmel, and G. Sapiro. Geodesic active contours. *International Journal of Computer Vision*, 22(1):61–79, Feb 1997. ISSN 0920-5691. doi: 10.1023/A:1007979827043.

T.F. Chan and L.A. Vese. Active contours without edges. *IEEE Transactions on Image Processing*, 10:266–277, 2001. ISSN 1047-3203.

C. Chang and C. Lin. LIBSVM: A library for support vector machines. *ACM Transactions on Intelligent Systems and Technology*, 2:27:1–27:27, 2011. Software available at http://www.csie.ntu.edu.tw/~cjlin/libsvm.